

Current-voltage characteristics of ZnSe-based Perovskite solar cells with inverted planar architecture

M. E. POPA

Department of Physical and Engineering Sciences, Alecu Russo Balti State University, Balti, MD-3100, Republic of Moldova

The work contains the experimental results obtained by applying of ZnSe thin films in perovskite solar cells. By using the ZnSe thin films as an electron transport layer (ETL) a maximum power conversion efficiency (PCE) of about 2.57 % was obtained. If we use a PC₆₁BM layer doped with ZnSe (1.4 mg/ml) as ETL, we get a maximum PCE of about 3.81 %. For perovskite solar cells with two ETL layers (ZnSe / PC₆₁BM) a maximum PCE of about 6.63 % was obtained. Solar cells with maximum efficiency of about 9.05% were obtained by doping the perovskite with ZnSe powder.

(Received September 23, 2019; accepted August 18, 2020)

Keywords: Perovskite, Selenide, Efficiency

1. Introduction

ZnSe is a chalcogenic semiconductor of the A^{II}B^{VI} family of semiconductor materials, that possesses a direct band gap of about 2.68-2.70 eV at room temperature [1-9]. In the form of thin layers it crystallizes in the form of cubics of the zinc-blend type, with a strong orientation of crystallite according to the plan (111) parallel to the support [1, 4-6]. The lattice parameter was estimated at the value $a = 5.658\text{-}5.667 \text{ \AA}$, and the interplanar distance $d_{111} = 3.260 - 3.270 \text{ \AA}$ [1, 4-6]. In the wavelength range 380-1080 nm the transmission coefficient of the ZnSe thin films is about 75-95%, the reflection coefficient does not exceed 0.5% [1-3, 5-7], and the edge of the absorption spectrum is about 2.25 eV [1, 3, 4, 7]. In these samples the refractive index varies from $n = 2.77$ (for $\lambda = 600 \text{ nm}$) to $n = 2.32$ (for $\lambda = 1720 \text{ nm}$) according to the law $n = 3.26732 - 0.00102\lambda + 2.69969 \times 10^{-7} \lambda^2$ [9]; the extinction coefficient decreases from $k = 0.044$ (for $\lambda = 600 \text{ nm}$) to $k = 0.017$ (for $\lambda = 1720 \text{ nm}$) [9], the real part of the dielectric constant decreases from $\epsilon_r = 7,7$ (for $\lambda = 600 \text{ nm}$) to $\epsilon_r = 5.4$ (for $\lambda = 1720 \text{ nm}$), and the imaginary part of the dielectric constant changes from $\epsilon_i = 0,24$ ($\lambda = 600 \text{ nm}$) to $\epsilon_i = 0,07$ (for $\lambda = 1720 \text{ nm}$) [9].

Due to the low absorption coefficient, excellent infrared transparency, high luminescence and increased sensitivity in the green-blue wavelength region, this material has multiple applications for the manufacture of optoelectronic devices such as light emitting diodes [10-14] lasers diodes [15] and optically controlled switching [16]. Various optical elements (windows, lenses, prisms) are prepared from zinc selenide, for the IR range, which are then used as laser optical elements.

Specialized literary resources contain the description of different techniques for the preparation of thin ZnSe layers, such as successive ionic layer adsorption and reaction (SILAR) method [17] electrodeposition [18-20],

chemical vapor deposition (CVD) [21-25], chemical solution [26], molecular beam epitaxy [27], RF sputtering [28] and thermal evaporation [1-9, 28, 29] for multiple applications in optoelectronic devices.

The wide band gap and high transparency in the visible field make ZnSe suitable for solar cell applications. P. Gashin et al. [30] have fabricated the tandem structure n-ZnSe/p-ZnTe/n-CdSe by successive epitaxial growth from the vapor phase of ZnTe and CdSe thin layers on ZnSe single crystals, and have obtained the efficiency of about 10.8%. F. Engelhardt et al. [31] have investigated Cu(In,Ga)Se₂-based solar cells with a ZnSe buffer layer deposited by metal-organic vapour and best solar cell achieving an efficiency of 11.6%. By spin-depositing poly(lauryl methacrylate) (PLMA) thin film doped with Mn:ZnSe quantum dots (QDs) on the front surface of Si solar cell for concentration $C_{QD} = 3.0 \text{ mg/ml}$. D. Ch. Cheng et al. [32] have achieved the highest efficiency at 9.97%. M. A. Olopade [33] has simulated Cu₂ZnSnS₄ solar cells with different buffer materials and has obtained the efficiency of 6.76% for cells with zinc selenide (ZnSe) as buffer layer. A. Rumberg et al. [34] have investigated polycrystalline ZnSe films as buffer layers in CIGSS based solar cells and have achieved the best efficiency of 9.6 %. P. Saikia et al. [35] have produced ZnSe/ZnTe/CdTe/HgTe multijunction solar cells on tin oxide coated glass substrate by the method of vacuum evaporation and these structures showed the best performance of photovoltaic parameters ($J_{sc} = 15.2 \text{ mA/cm}^2$; $V_{oc} = 765 \text{ mV}$; $FF = 65.05\%$; $\eta = 9.86\%$).

In recent years, a great deal of interest has attracted different perovskite materials for applications in solar cells. In specialized articles [36-45] it has been demonstrated that perovskite solar cells can achieve significantly higher conversion efficiency of electricity compared to standard silicon cells and other thin-layered cells and can reduce production costs. Some metal sulfides

have recently been investigated as electron transport layer in perovskite devices [46-47]. Zinc selenide (ZnSe) is a potential material for multiple applications in various nanostructures.

The purpose of this paper is to present the obtained results in the use of ZnSe thin films as electron transport layer and dopant in perovskite ($\text{CH}_3\text{NH}_3\text{PbI}_3$) solar cells.

2. Experimental section

The thin layer of indium tin oxide (ITO) was deposited by engraving on Corning 7059 glass that was later cleaned by ultrasonic detergent, deionized water, acetone, methanol and isopropanol for the function of electrode that collects holes.

The PEDOT-PSS (poly (3,4-ethylenedioxy thiophene) - poly (styrene sulfonate)) layer, which has the function of the hole transport layer, was deposited on ITO. This is, usually, deposited from a solution (80 μl) by the spin-coating method at a rotational speed of 3000 rpm for 60 seconds followed by heat treatment in the air for 10 minutes at the temperature of 150°C. The time of the treatment is measured by the phone chronometer.

The solution of perovskite $\text{CH}_3\text{NH}_3\text{PbI}_3$ (methylammonium lead iodide) was used for the

preparation of bulk heterojunction. The perovskite layer is deposited from the solution (80 μl) by the two-stage spin coating process: after depositing for 23 seconds the layer is rotated at 1000 rpm, followed by a second deposition for 30 seconds at a speed of 4000 rpm. At the 13th second 150 μl of toluene is dripped.

For the function of electron transport layer a ZnSe layer with an evaporation mass of about 32 mg of ZnSe powder is deposited at the temperature of the glass substrate $T_{sub} = 300\text{K}$ by vacuum thermal evaporation. The vacuum pressure is about 72×10^{-4} torr, and the electrical current through the evaporator is approximately 50 A. The Ag electrodes are deposited analogously by thermal evaporation in quasi-closed volume.

A layer deposited from 60 μl solution of PCBM = PC_{61}BM (fullerene derivate [6,6] -phenyl-C61-butyric acid methylester) doped with ZnSe was used as the transport electron layer in another type of solar cell. The layer was deposited through dynamic dispensing (in g-box) spin-coating in the argon chamber at a rotation speed of 1000 rpm for 40 s. It was found that the most successful solar cell was at the concentration of 1.4 mg of ZnSe in one ml of PC_{61}BM . The other layers were deposited as in the previous cells.

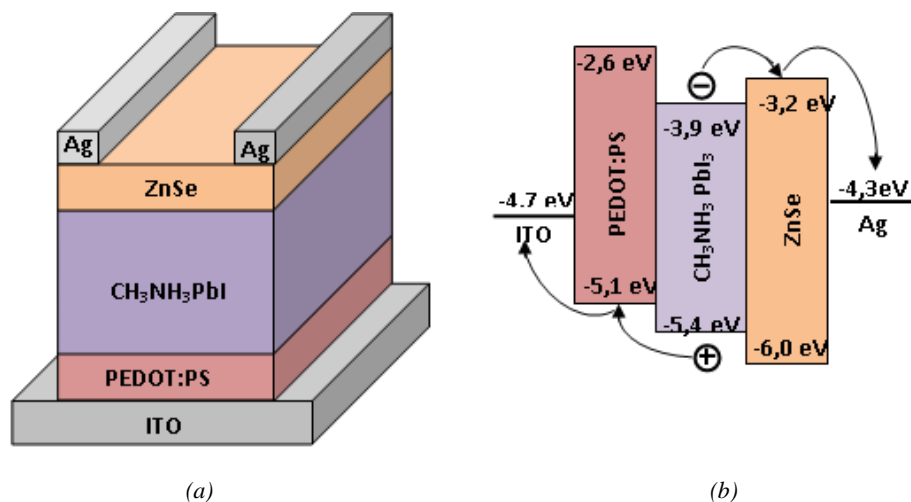


Fig. 1. (a) Device structure of inverted planar architecture of perovskite solar cells; (b) The energy diagram of inverted planar perovskite solar cells (color online)

Two layers of electron transport layer type have been deposited in the third variant of solar cells: the first layer of ZnSe was deposited by vacuum thermal evaporation under the same conditions as in the first variant of solar cells; the second layer of PC_{61}BM was deposited through dynamic dispense (in g-box) spin-coating in the argon chamber at a rotation speed of 1000 rpm for 40 s. The other layers were deposited as in the previous cells.

In the fourth variant of solar cells, the bulk heterojunction layer is obtained from ZnSe-doped perovskite ($\text{CH}_3\text{NH}_3\text{PbI}_3$) solution. The deposition was carried out similarly as in depositing perovskite without

impurities. It was found that the most successful solar cell of this kind was obtained for the concentration of 1.6 mg of ZnSe in one ml of $\text{CH}_3\text{NH}_3\text{PbI}_3$. The other layers have been deposited as in previous devices.

The current density-voltage curves of the devices were measured in a N_2 filled glove box using simulated AM1.5G sun light which was calibrated to $100\text{mW}/\text{cm}^2$ using a NREL traceable Si photodiode (PV Measurements Inc.) and a Keithley 2400 source measurement unit controlled by a PC. The photovoltaic parameters of the multijunction solar cells were investigated at 300 K. The surface morphology of the solar cells was observed using

the scanning electron microscope (SEM) type VEGA3 TESCAN and HITACHI S-3000N.

3. Results and discussions

The process of converting the solar energy into electrical energy at the level of the solar cell takes place in several stages. At illumination of a solar cell, the photons, whose energy is greater than the width bandgap of the main absorber, are absorbed and produce excitons which diffusing in the bulk of absorber they can meet sites of dissociation and then the electrons and holes will be produced. Further these can be separated by the driving forces present at the interface D/A spread the whole volume of bulk heterojunction cell or by the built electric field present at the p-n interfaces in a bilayered or

multilayered structure, giving rise finally to the photogenerated charge carriers (electrons and holes) collected to the electrodes and participating to the photovoltaic response.

Usually, the solar cell has a sandwich structure, in which the perovskite layer is located between the electron transport layer and the hole transport layer. Fig. 1.a. presents the cascade structure of a solar cell with inverted planar architecture in which ZnSe plays the role of electron transport layer, and the PEDOT: PSS layer plays the role of hole transport layer. Fig. 1.b presents the energy diagram of the ITO/PEDOT: PSS/CH₃NH₃PbI₃/ZnSe/Ag cell. It is noted that in this structure the hole passes the energy route -5.4 eV → -5.1 eV → -4.7 eV while the electron passes the energy route -3.9 eV → -3.2 eV → -4.5 eV.

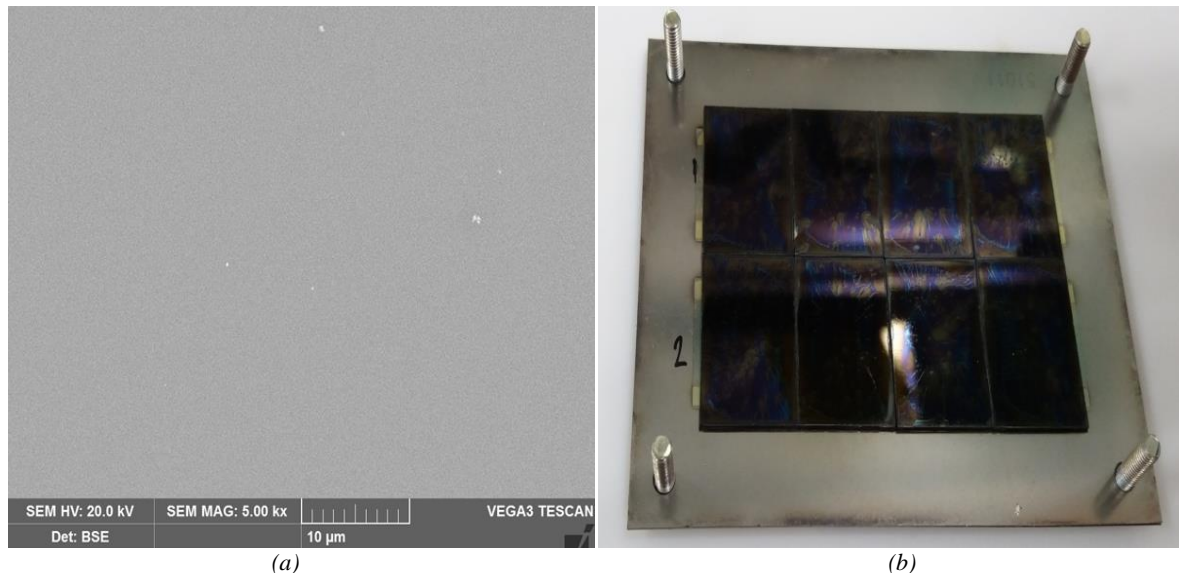


Fig. 2. (a) SEM image of ZnSe thin films from perovskite solar cells; (b) Photo of ITO/PEDOT:PSS/CH₃NH₃PbI₃/ZnSe/Ag thin cells (color online)

Fig. 2 a presents the SEM image of the ITO/PEDOT:PSS/CH₃NH₃PbI₃/ZnSe/Ag cell. It is noted that the surface has very small crystallites, and the size and shape of crystallites are similar. However, in some places some small irregular shaped grains appear on the surface; they probably represent some pieces of powder, which have not got crystallized at the surface. Fig. 2 b presents a photo of the samples, made before the deposition of silver electrodes. It is observed that the layers are uniform and have the same color.

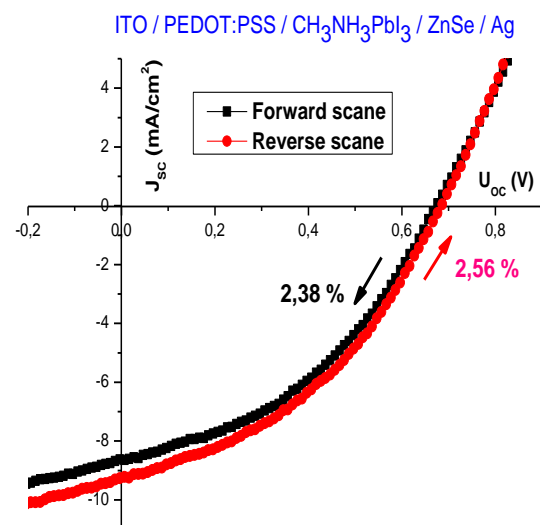


Fig. 3. Current density – voltage characteristics of perovskite solar cells with ZnSe as electron transport layer (color online)

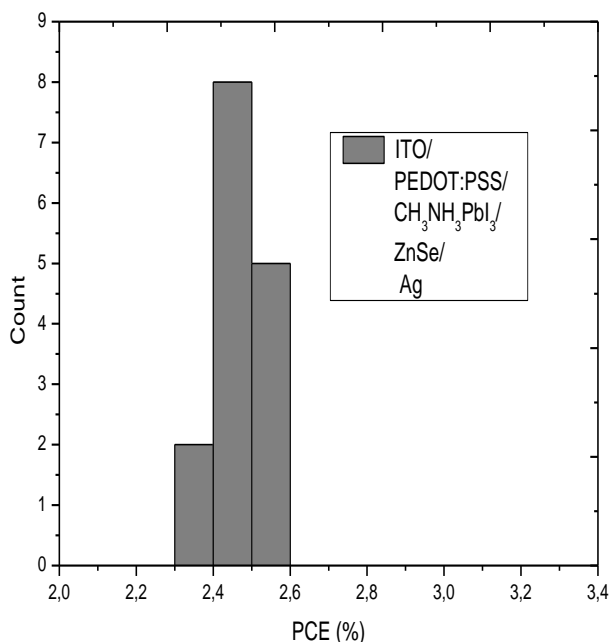


Fig. 4. Histograms of PCEs of perovskite solar cells with ZnSe as electron transport layer

Table 1. Photovoltaic parameters of ITO/PEDOT:PSS/CH₃NH₃PbI₃/ZnSe/Ag thin solar cells

Direction of scan	U _{oc} (V)	J _{sc} (mA/cm ²)	FF(%)	PCE (%)
Forward	0.677	-8.627	40.315	2.379
Reverse	0.687	-9.266	40.758	2.565

In Fig. 3 we can see the current density - voltage curves of the most representative solar ITO/PEDOT:PSS/CH₃NH₃PbI₃/ZnSe/Ag cell at forward scanning (at voltage increase) and reverse scanning (at voltage decrease) and Table 1 presents the values of the photovoltaic parameters of the respective solar cells. We notice that curve hysteresis is almost similar, and the values of photovoltaic parameters are insignificantly changed. At forward scanning we obtain an open circuit voltage $V_{oc} = 0.677$ V, the short-circuit current $J_{sc} = -8.627$ mA/cm², the fill factor $FF = 40.315$ % and the power conversion efficiency $PCE = 2.379$ %. At reverse scanning we get slightly higher values ($V_{oc} = 0.687$ V, $J_{sc} = -9.266$ mA/cm², $FF = 40.758$ %, $PCE = 2.565$ %) (Table 1).

In Fig. 4 we can see the histogram of fifteen solar cells of the type ITO/PEDOT:PSS/CH₃NH₃PbI₃/ZnSe/Ag measured at forward voltage scanning. We can notice that five devices have energy efficiency ranging from 2.5%, to 2.6%, eight devices have energy efficiency between 2.4% and 2.5% and only two devices have energy efficiency from 2.3% to 2.4%.

In another variant of solar cells, the PC₆₁BM layer doped with ZnSe was used as the electron transport layer, and the other solar cell components were prepared similarly to the previous samples. In Fig. 5 we can see J-U curves of the most efficient solar cell type ITO/PEDOT:PSS/CH₃NH₃PbI₃/PC₆₁BM:ZnSe/Ag at forward scanning (at voltage decrease) and reverse

scanning (at voltage increase) and Table 2 presents the values of the photovoltaic parameters of the respective cells. We notice that the curve hysteresis of the reverse scanning is smaller than the forward scanning, and the photovoltaic parameter values are as follows: the open circuit voltage (V_{oc}) remains constant at 0.727 V, the short-circuit current (J_{sc}) increases from 10.046 mA/cm² to 10.131 mA/cm², while the fill factor (FF) decreases from 52.212% to 48.518%, and the power conversion efficiency (PCE) evolves from 3.812% to 3.572%.

In Fig. 6 we see a histogram of fifteen solar cells of the type ITO/PEDOT:PSS/CH₃NH₃PbI₃/PC₆₁BM:ZnSe/Ag measured at forward voltage scanning. It is noticed that four devices have an energy efficiency of 3.75 – 3.85%, seven devices have an energy efficiency of 3.65 – 3.75%, and the other four devices have an energy efficiency of 3.55 – 3.65%.

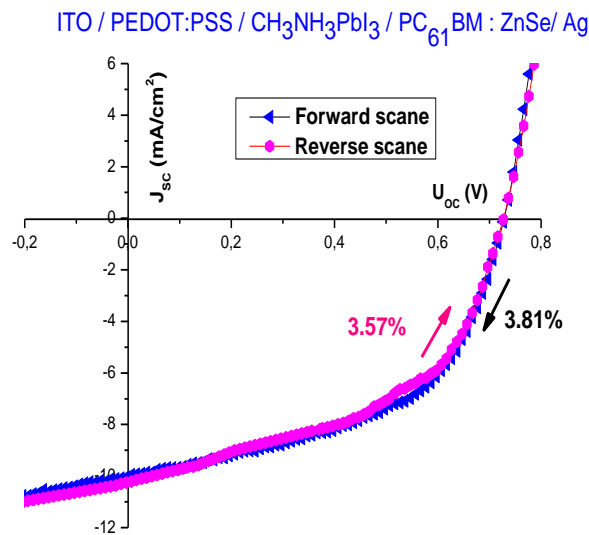


Fig. 5. J – U curves of perovskite solar cells with PC₆₁BM:ZnSe as electron transport layer (color online)

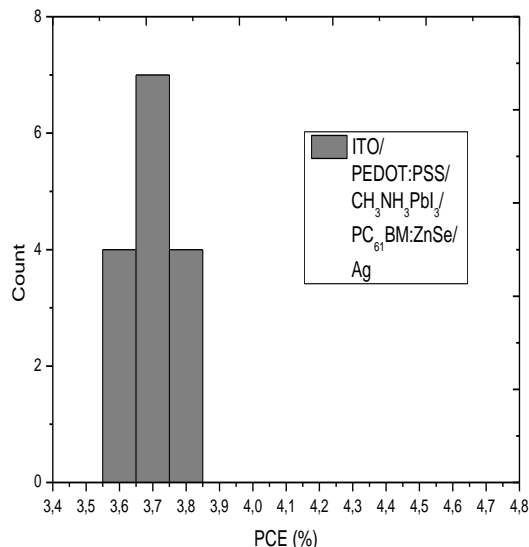


Fig. 6. Histograms of PCEs of perovskite solar cells with PC₆₁BM:ZnSe as electron transport layer

Table 2. Photovoltaic parameters of ITO/PEDOT:PSS/CH₃NH₃PbI₃/PC₆₁BM:ZnS/Ag thin solar cells

Direction of scan	U _{oc} (V)	J _{sc} (mA/cm ²)	FF(%)	PCE (%)
Forward	0.727	-10.046	52.212	3.812
Reverse	0.727	-10.131	48.518	3.572

The third variant of the solar cell contains two layers of electron transfer layer: one of ZnSe and the second of PC₆₁BM. Fig. 7 represents current density- voltage curves of the most representative type of solar cell: ITO/PEDOT:PSS/CH₃NH₃PbI₃/ZnSe/PC₆₁BM/Ag at forward scanning (at lowering voltage) and reverse scanning (when the voltage increases). Table 3 presents the values of the photovoltaic parameters of the respective cells. We notice that curve hysteresis is almost similar, and the values of the photovoltaic parameters evolve in the following way: the open circuit voltage (V_{oc}) decreases from 0.927 V to 0.917 V, the short-circuit current (J_{sc}) decreases from -13.207 mA/cm² to -12.667 mA/cm², the fill factor (FF) increases from 54.157 % to 56.039 % and the value of power conversion efficiency (PCE) changes from 6.628% to 6.508%.

In Fig. 8. we see the energy diagram of ITO/PEDOT:PSS/CH₃NH₃PbI₃/ZnSe/ PC₆₁BM /Ag solar cells. We notice that this structure simplifies the electron trace from the perovskite to the Ag electrode by making small drops in the cascade between the closer energy levels (from - 3.9 eV to - 3.2 eV, then to - 4.3 eV to - 4.5 eV). This one, probably, explains the growth of the PCE value of the respective cells compared to other devices.

In Fig. 9 we see the histogram of fifteen solar cells of the type ITO/PEDOT:PSS/CH₃NH₃PbI₃/ZnSe/ PC₆₁BM/Ag measured at forward voltage scanning. It is noticed that four devices have an energy efficiency of 6.6 – 6.7 %, eight devices have an energy efficiency of 6.5 – 6.6 %, and the other three devices have an energy efficiency of 6.4 – 6.5 %.

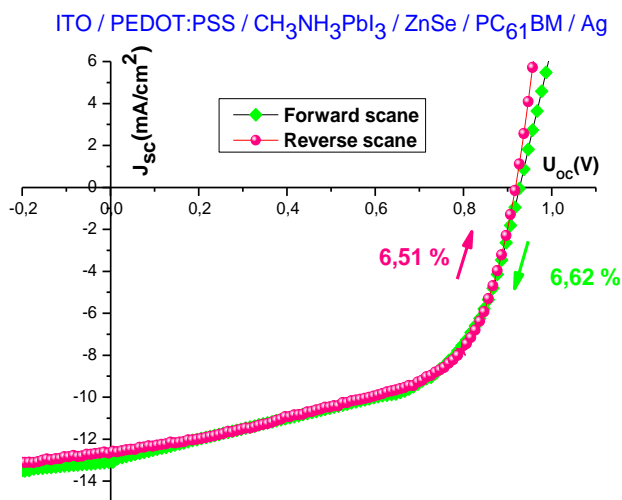


Fig. 7. *J – U* curves of perovskite solar cells with ZnSe/PC₆₁BM as double electron transport layer (color online)

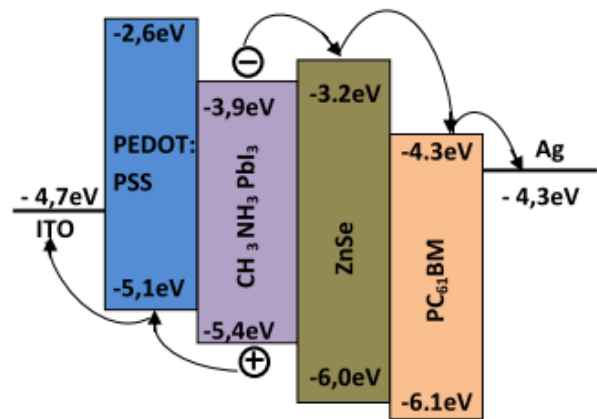


Fig. 8. The energy diagram of ITO/PEDOT:PSS/CH₃NH₃PbI₃/ZnSe/PC₆₁BM/Ag thin solar cells (color online)

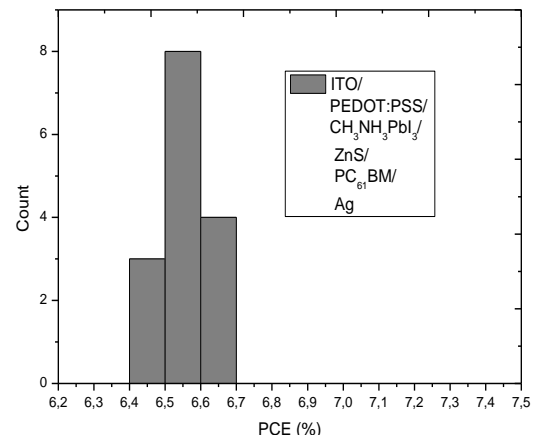


Fig. 9. Histograms of PCEs of perovskite solar cells with ZnSe/PC₆₁BM as double electron transport layer

Table 3. Photovoltaic parameters of ITO/PEDOT:PSS/CH₃NH₃PbI₃/ZnSe/PC₆₁BM/Ag thin solar cells

Direction of scan	U _{oc} (V)	J _{sc} (mA/cm ²)	FF(%)	PCE (%)
Forward	0.927	-13.207	54.157	6.628
Reverse	0.917	-12.667	56.039	6.508

In the fourth variant of solar cells the bulk heterojunction layer was obtained by doping perovskite CH₃NH₃PbI₃ with ZnSe powder. For functional devices with the best photovoltaic characteristics, the concentration of the powder in the solution was of 1.6 mg/ml. The deposition conditions of the doped layer were the same as in the case of the deposition of the pure perovskite layer.

Fig. 10 shows the SEM image of a solar cell of the type ITO/PEDOT:PSS/CH₃NH₃PbI₃/ZnSe/ PC₆₁BM/ Ag. It is seen that the surface is uniform with small formations of different shapes. In Fig. 11 we see a sample photograph taken after the deposition of silver electrodes. It is noted that the layers are uniform and have the same color.

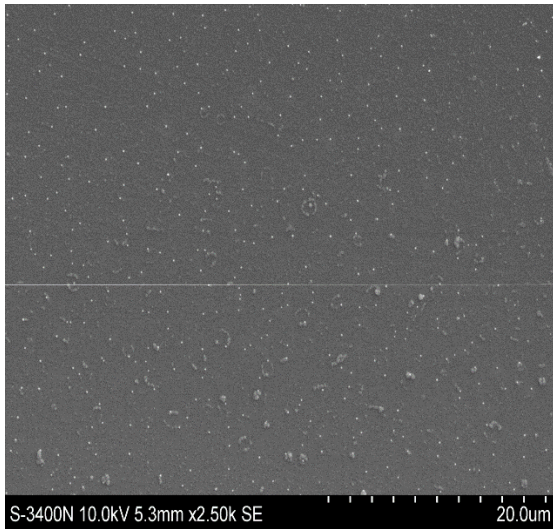


Fig. 10. SEM image of PC₆₁BM thin films from perovskite solar cells

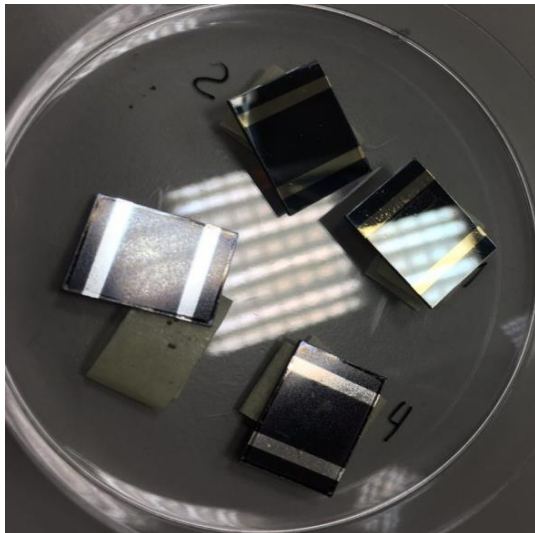


Fig. 11. Photo of ITO/PEDOT:PSS/ CH₃NH₃PbI₃: ZnSe/PC₆₁BM /Ag thin cells (color online)

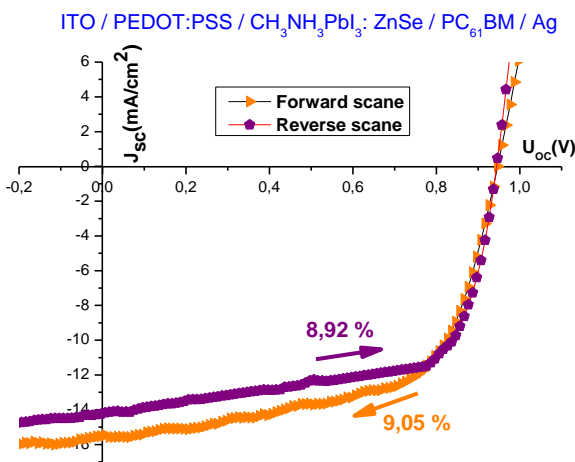


Fig. 12. Current density – voltage characteristics of perovskites solar cells doped with ZnSe (color online)

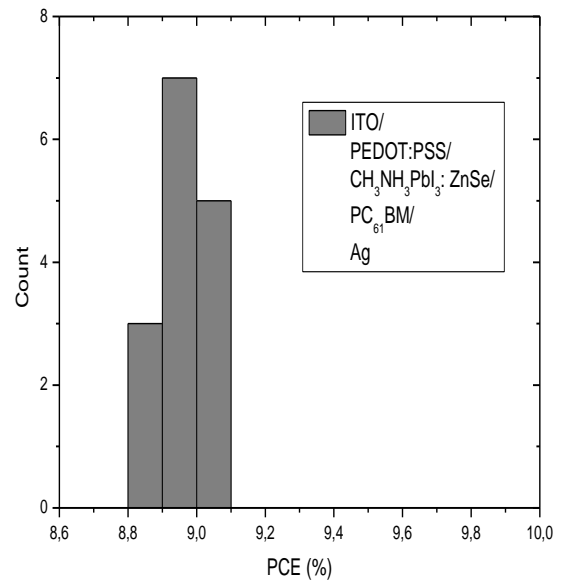


Fig. 13. Histograms of PCEs for solar cells type ITO/PEDOT:PSS/ CH₃NH₃PbI₃:ZnSe/PC₆₁BM/Ag

Table 4. Photovoltaic parameters of ITO/PEDOT:PSS/CH₃NH₃PbI₃:ZnSe/PC₆₁BM /Ag thin solar cells

Direction of scan	U _{oc} (V)	J _{sc} (mA/cm ²)	FF(%)	PCE (%)
Forward	0.947	-15.521	61.556	9.047
Reverse	0.947	-14.292	65.878	8.916

Fig. 12 shows the current density-voltage curves for the best-performing solar cell of the type ITO/PEDOT:PSS/CH₃NH₃PbI₃:ZnSe/PC₆₁BM/Ag. At forward scanning, it had an open circuit voltage (V_{oc}) of 0.947 V, a short circuit current (J_{sc}) of -15.521 mA/cm², a fill factor (FF) of 61.556% and a power conversion efficiency of 9.047%. At reverse scanning, the following characteristics were obtained: V_{oc} = 0.947 V, J_{sc} = -14.292 mA/cm², FF = 65.878 % and PCE of 8.916 %.

In Fig. 13 we see the histogram of fifteen solar cells of the type ITO/PEDOT:PSS/ CH₃NH₃PbI₃:ZnSe/PC₆₁BM/Ag measured at forward voltage scanning. It is noticed that five devices have energy efficiency of 9.0 – 9.1 %, seven devices have energy efficiency of 8.9 – 9.0%, and the other three devices have energy efficiency ranging from 8.8% to 8.9%.

In specialized literature sources there are only publications on the application of zinc sulphide in perovskite structures. In the paper [46] an analogue cascade structure was described in which the electron transport layer of the solar cell consists of two thin layers: one of ZnS and one of TiO₂, resulting in an efficient conversion of 4.90% at forward scanning and 5.27% at reverse scanning. Jiang Liu et al. [47] prepared solar cells of the ITO/ZnS/perovskite/spiro-OMeTAD/Au type, achieving an efficient conversion of 0.98%. Mihail Popa et al. [48] demonstrated the application of ZnS thin layers in

the perovskite solar cells. By using two electron transport layers, one of PC₆₁BM and second of ZnS, solar cells with a maximum power conversion efficiency of about 5.76% were obtained.

Given the high coefficient of extinction of perovskites, the inverted planar architecture devices proposed here represent a new project for excitonic photovoltaic devices without a mesoscopic structure. II-VI semiconductor based on solar cells are among the most important candidates for photovoltaic conversion with low solar energy and reduced costs due to their high absorption coefficients and hence low consumption of material for their production.

4. Conclusions

1. The paper has demonstrated the use of various structures of zinc selenide as an electron transport layer or as a dopant in perovskite solar cells with inverse planar architecture. The advantages of these cells would be their preparation at low temperatures by two relatively cheap methods: spin-coating and thermal evaporation.

2. The efficiencies of the investigated structures are good for the third generation of the solar cells including (in the last 5-10 years) the perovskite solar cells, (but unfortunately nonstabilized yet), the results obtained are important from technological point of view, showing a new way to improve the performances of the photovoltaic cells based perovskite.

References

- [1] M. Popa, I. Tiginyanu, P. Topala, V. Ursaki, *Nanostructures and Thin Films for Multifunctional Applications: Technology, Properties and Devices*, Springer, 115 (2016).
- [2] G. I. Rusu, M. E. Popa, G. G. Rusu, Iulia N. Salaoru, *Appl. Surf. Sci.* **218**(1-4), 213 (2003).
- [3] M. E. Popa, G. I. Rusu, *Phys. Low-Dim. Struct* **7**(8), 43 (2003).
- [4] G. I. Rusu, V. Ciupina, M. E. Popa, G. Prodan, G. G. Rusu, C. Baban, *J. Non-Cryst. Solids* **352**, 1525 (2006).
- [5] G. I. Rusu, M. Diciu, C. Pîrghie, M. E. Popa, *Appl. Surf. Sci.* **253**, 9500 (2007).
- [6] M. E. Popa, G. I. Rusu, *Optoelectron. Adv. Mat.* **5**(8), 842 (2011).
- [7] M. E. Popa, *Rom. Rep. Phys.* **68**(4), 1495 (2016).
- [8] M. Popa, I. Tiginyanu, V. Ursaki, *Rom. J. Phys.* **62**(1-2), 1 (2017).
- [9] M. Popa, I. Tiginyanu, V. Ursaki, *Mold. J. Phys. Sci.* **16**(1-2), 78 (2017).
- [10] T. Shirakawa, *Mater. Sci. Ebg. B Adv.* **91-92**, 470 (2002).
- [11] D. S. Patil, D. K. Gautam, *Opt. Commun.* **201**, 413 (2002).
- [12] T. Nakamura, K. Katayama, H. Mori, S. Fujiwara, *Phys. Stat. Sol. B* **241**(12), 2659 (2004).
- [13] S. Venkatachalam, R. T. Rajendra Kumar, D. Mangalaraj, Sa. K. Narayandass, Kyunghae Kim, Junsin Yi, *Solid-State Electron.* **48**, 2219 (2004).
- [14] Yuji Araki, Koji Ohkuno, Takeshi Furukawa, Junji Saraie, *J. Cryst. Growth* **301-302**, 809 (2007).
- [15] S. V. Ivanov, E. V. Lutsenko, S. V. Sorokin, I. V. Sedova, S. V. Gronin, A. G. Voinilovich, N. P. Tarasuk, G. P. Yablonskii, P. S. Koptev, *J. Cryst. Growth* **311**, 2120 (2009).
- [16] M. Woodford, K. F. MacDonald, G. C. Stevens, N. I. Zheludev, *Opt. Commun.* **254**, 340 (2005).
- [17] R. B. Kale, C. D. Lokhande, *Mater. Res. Bull.* **39**, 1829 (2004).
- [18] C. Natarajan, M. Sharon, C. Levy-Clement, M. Neumann-Spallart, *Thin Solid Films* **237**, 118 (1994).
- [19] K. R. Murali, S. Dhanapandiyana, C. Manoharana, *Chalcogenide Lett.* **6**(1), 51 (2009).
- [20] D. Saravanakumar, M. Kashif, V. Rethinasami, B. Ravikumar, S. Pandiarajan, A. Ayeshamariam, A. Sivaranjani, M. Bououdina, S. Ramalingam, *J. Ovonic Res.* **10**(5), 175 (2014).
- [21] J. M. Dona, J. Herrero, *J. Electrochem. Soc.* **142**(3), 764 (1995).
- [22] C. D. Lokhande, P. S. Patil, H. Tributsch, A. Ennaoui, *Sol. Energ. Mat. Sol. C* **55**, 379 (1998).
- [23] P. C. Pingale, S. T. Mane, R. V. Suryawanshi, L. P. Deshmukh, *Adv. Appl. Sci. Res.* **4**(3), 177 (2013).
- [24] B. G. Durdu, U. Alver, A. Kucukonder, Ö. Söğüt, M. Kavgac, *Acta Phys. Pol. A* **124**(1), 41 (2013).
- [25] S. Sagadevan, I. Das, *Aust. J. Mech. Eng.* **15**(3), 222 (2016).
- [26] L. Chen, C. Fang, *Appl. Mech. Mater.* **321-324**, 264 (2013).
- [27] T. Yao, M. Ogura, S. Matsuoka, T. Morishita, *Appl. Phys. Lett.* **43**, 499 (1983).
- [28] V. Mittal, N. P. Sessions, J. S. Wilkinson, G. S. Murugan, *Opt. Mater. Express* **7**(3), 712 (2017).
- [29] J. Sharma, D. Shikha, S. K. Tripathi, *Rom. Rep. Phys.* **66**(4), 1002 (2014).
- [30] P. Gashin, A. Focsha, T. Potlog, A. V. Simashkevich, V. Leonard, *Sol. Energ. Mat. Sol. C* **46**, 323 (1997).
- [31] F. Engelhardt, L. Bornemann, M. Koentges, Th. Meyer, J. Parisi, E. Pschorr-Schoberer, B. Hahn, W. Gebhardt, W. Riedl, U. Rau, *Prog. Photovoltaics* **7**, 423 (1999).
- [32] D. C. Cheng, H. C. Hao, M. Zhang, W. Shi, M. Lu, *Nanoscale Res. Lett.* **8**, 291 (2013).
- [33] M. A. Olopade, O. O. Oyebola, B. S. Adeleke, *Adv. Appl. Sci. Res.* **3**(6), 3396 (2012).
- [34] A. Rumberg, Ch. Sommerhalter, M. Toplak, A. Jager-Waldau, M. Ch. Lux-Steiner, *Thin Solid Films* **361-362**, 172 (2000).
- [35] P. Saikia, P. K. Saikia, D. Saikia, *Optoelectron. Adv. Mat.* **5**(3), 204 (2011).
- [36] J. H. Im, Ch. R. Lee, J. W. Lee, S. W. Park, N. G. Park, *Nanoscale* **3**, 4088 (2011).
- [37] M. M. Lee, J. Teuscher, T. Miyasaka,

- T. N. Murakami, H. J. Snaith, *Science* **338**, 643 (2012).
- [38] J. Y. Jeng, Y. F. Chiang, M. H. Lee, S. R. Peng, T. F. Guo, P. Chen, T. C. Wen, *Adv. Mater.* **25**(27), 3727 (2013).
- [39] B. Conings, L. Baeten, C. De Dobbelaere, J. D'Haen, J. Manca, H. G. Boyen, *Adv. Mater.* **26**(13), 2041 (2013).
- [40] S. D. Stranks, G. E. Eperon, G. Grancini, C. Menelaou, M. J. P. Alcocer, T. Leijtens, L. M. Herz, A. Petrozza, H. J. Snaith, *Science* **341**, 342 (2013).
- [41] W. J. Yin, T. Shi, Y. Yan, *Adv. Mater.* **26**(27), 4653 (2014).
- [42] Q. Lin, A. Armin, R. Chandra, R. Nagiri, P. L. Burn, P. Meredith, *Nat. Photonics* **9**, 106 (2014).
- [43] N. J. Jeon, J. H. Noh, Y. Ch. Kim, W. S. Yang, S. Ryu, S. I. Seok, *Nat. Mater.* **13**, 897 (2014).
- [44] W. J. Yin, T. Shi, Y. Yan, *J. Phys. Chem. C* **119**(10), 5253 (2015).
- [45] V. A. Milichko, A. S. Shalin, I. S. Mukhin, A. E. Kovrov, A. A. Krasilin, A. V. Vinogradov, P. A. Belov, C. R. Simovskii, *Phys.-Uspekhi* **186**(8), 801 (2016).
- [46] W. Ke, C. C. Stoumpos, J. L. Logsdon, M. R. Wasielewski, Y. Yan, G. Fang, M. G. Kanatzidis, *J. Am. Chem. Soc.* **138**, 14998 (2016).
- [47] J. Liu, C. Gao, L. Luo, Q. Ye, X. He, L. Ouyang, X. Guo, D. Zhuang, C. Liao, J. Mei, W. Lau, *J. Mater. Chem. A* **3**, 11750 (2015).
- [48] M. Popa, A. Zakhidov, I. Tiginyanu, *P. Romanian Acad. A* **19**(4), 559 (2018).

* Corresponding author: miheugpopa@yahoo.com